

Two-dimensional room temperature ferromagnetic semiconductors

Jia-Wen Li,¹ Gang Su,^{1,2,3,4,*} and Bo Gu^{1,2,†}

¹*Kavli Institute for Theoretical Sciences, University of Chinese Academy of Sciences, Beijing 100049, China*

²*Physical Science Laboratory, Huairou National Comprehensive Science Center, Beijing 101400, China*

³*School of Physical Sciences, University of Chinese Academy of Sciences, Beijing 100049, China*

⁴*Institute of Theoretical Physics, Chinese Academy of Sciences, Beijing 100190, China*

To realize ferromagnetic semiconductors with high Curie temperature T_C is still a challenge in spintronics. Recent experiments have obtained two-dimensional (2D) room temperature ferromagnetic metals, such as monolayers MnSe_2 and Cr_3Te_6 . In this paper, by the density functional theory (DFT) calculations, we proposed a way to obtain 2D high T_C ferromagnetic semiconductors through element replacement in these ferromagnetic metals. High T_C ferromagnetic semiconductors are predicted in the monolayers $(\text{Mn}, \text{D})\text{Se}_2$ and $(\text{Cr}, \text{D})_3\text{Te}_6$, where element D is taken as vacancy, 3d, 4d and 5d transition metal elements. For the concentrations of D from 1/9 to 1/3, there are about 10 ferromagnetic semiconductors with T_C above 200 K, including $(\text{Cr}_{5/6}, \text{W}_{1/6})_3\text{Te}_6$ and $(\text{Cr}_{4/6}, \text{Mo}_{2/6})_3\text{Te}_6$ with T_C above 300 K. In addition, $\text{Mn}(\text{Se}_{6/8}, \text{Sb}_{2/8})_2$ is also predicted to be a 2D ferromagnetic semiconductor with T_C above 300 K. Considering the fast developments on fabrication and manipulation of 2D materials, our theoretical results propose a way to explore the high temperature ferromagnetic semiconductors from experimentally obtained 2D high temperature ferromagnetic metals through element replacement approach.

Introduction.—Due to the interesting properties, there are many promising applications of magnetic semiconductors [1–20], such as spin injection maser [19, 20], circular polarized light emitting diodes [10], magnetic diode and p-n junction [11–15], magnetic tunnel junction [16, 17], and spin valve structures [18], etc. These applications require magnetic semiconductors with high Curie temperature T_C above room temperature. However, the T_C of ferromagnetic semiconductors show low T_C far below room temperature, largely limit their applications.

The intrinsic three-dimensional ferromagnetic semiconductors in nature show low T_C [21]. In 2017, the successful synthesis of two-dimensional (2D) van der Waals ferromagnetic semiconductors CrI_3 [22] and $\text{Cr}_2\text{Ge}_2\text{Te}_6$ [23] in experiments has attracted extensive attentions to 2D ferromagnetic semiconductors. According to Mermin-Wagner theorem [24], the magnetic anisotropy is essential to produce long-range magnetic order in 2D systems. Recently, more 2D ferromagnetic semiconductors have been obtained in experiments, such as Cr_2S_3 [25], CrCl_3 [26], CrBr_3 [27], CrSiTe_3 [28] and CrSBr [29], where the T_C are far below room temperature. In addition, many ferromagnetic semiconductors with T_C above room temperature have been predicted based on theoretical calculations [30–39], while their synthesis remains a challenge.

On the other hand, the 2D van der Waals ferromagnetic metals with high T_C have been obtained in recent experiments. For example, $T_C = 140$ K in CrTe [40], 300 K in CrTe_2 [41–43], 344 K in Cr_3Te_6 [44], 160 K in Cr_3Te_4 [45], 280 K in CrSe [46], 300 K in Fe_3GeTe_2 [47, 48], 270 K in Fe_4GeTe_2 [49], 229 K in Fe_5GeTe_2 [50], 380 K in Fe_3GaTe_2 [51, 52], 300 K in MnSe_2 [53], etc.

Doping is a widely used method to control properties of 2D materials [30, 54–65]. In addition to the extensive

studies of the diluted magnetic semiconductors by doping in 3D non-magnetic semiconductors [5, 6], there are some recent efforts to obtain 2D ferromagnetic semiconductors by doping in 2D non-magnetic semiconductors [54–57, 63, 64]. There are also some theoretical studies on the magnetic properties of the 2D doped materials [58–62, 66]. In addition, doping can also induce metal-semiconductor transitions in 2D metals, as reported in recent experiments [52, 65, 67, 68], and theoretical studies [66, 69, 70].

In contrast to the conventional diluted magnetic semiconductors by doping magnetic impurities into non-magnetic semiconductors, is it possible to obtain magnetic semiconductors by doping impurities into magnetic metals? Inspired by the recent experimental and theoretical progress of 2D materials, we argue that it becomes possible in 2D systems. Because two important conditions are satisfied in 2D systems now. First, the 2D ferromagnetic metals with high T_C . It is satisfied with the help of great progress of 2D ferromagnetic metals in recent experiments. Second, the doping-induced metal-semiconductor transitions. It is also possible in 2D metals as reported in the recent experimental and theoretical studies.

In this letter, we demonstrate the above idea to predict the ferromagnetic semiconductors with high T_C through element replacement in 2D ferromagnetic metals. For our purpose, the 2D ferromagnetic metals MnSe_2 with $T_C = 300$ K and Cr_3Te_6 with $T_C = 344$ K reported in recent experiments [44, 53] are chosen as host metals. By density functional theory (DFT) calculations, the properties of monolayers $(\text{Mn}_{1-x}, \text{D}_x)\text{Se}_2$ and $(\text{Cr}_{1-x}, \text{D}_x)_3\text{Te}_6$ are studied, where D are vacancy, 3d, 4d and 5d transition metal elements, x is concentration of D. For x from 1/9 to 1/3, we have predicted about 10 ferromagnetic semi-

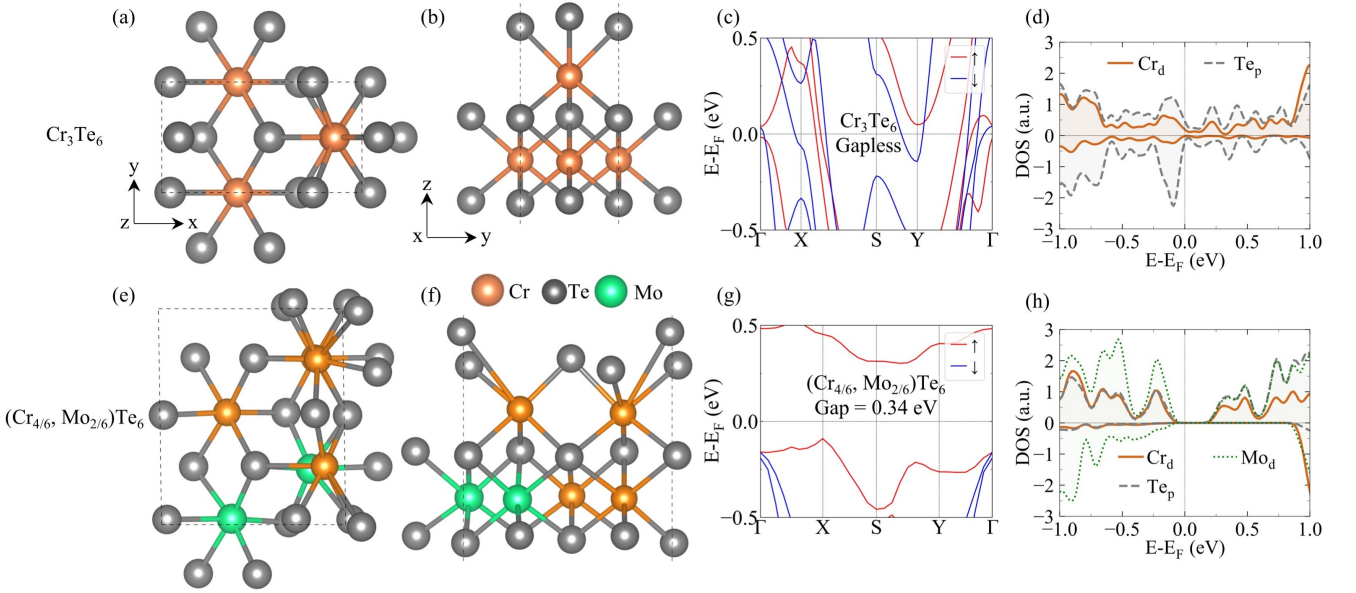


FIG. 1. Crystal structures and band structures, partial density of state (PDOS) of monolayers Cr_3Te_6 and $(\text{Cr}_{4/6}, \text{Mo}_{2/6})_3\text{Te}_6$. (a) Top view and (b) side view of monolayer Cr_3Te_6 . (c) Spin polarized band structure of Cr_3Te_6 . (d) Spin polarized partial density (PDOS) of monolayer Cr_3Te_6 . (e) Top view and (f) side view of monolayer $(\text{Cr}_{4/6}, \text{Mo}_{2/6})_3\text{Te}_6$. (g) Spin polarized band structure of $(\text{Cr}_{4/6}, \text{Mo}_{2/6})_3\text{Te}_6$, showing a band gap of 0.34 eV. (h) Spin polarized PDOS of monolayer $(\text{Cr}_{4/6}, \text{Mo}_{2/6})_3\text{Te}_6$. The band structures are obtained by the DFT calculation with HSE functional.

conductors with T_C above 200 K, i.e., $(\text{Mn}_{6/9}, \text{D}_{3/9})\text{Se}_2$ with D as Mn vacancy, Au and Cd, $(\text{Cr}_{4/6}, \text{D}_{2/6})_3\text{Te}_6$ with D as Ag, Hg and Mo. Their stability and feasibility of element replacement are confirmed by the calculations of formation energy, defect formation energy and molecular dynamics simulations. As an example, property of $(\text{Cr}_{4/6}, \text{Mo}_{2/6})_3\text{Te}_6$ with $T_C = 400$ K and band gap of 0.34 eV is discussed in detail in the paper, and others are given in the Supplemental Material [71]. Our theoretical results propose a way to obtain high temperature ferromagnetic semiconductors by element replacement in 2D ferromagnetic metals in experiments.

Properties of monolayers Cr_3Te_6 and $(\text{Cr}_{4/6}, \text{Mo}_{2/6})_3\text{Te}_6$.—The top and side views of crystal structure of monolayer Cr_3Te_6 are shown in Figs. 1(a) and 1(b), respectively, with a space group Pm (No. 6). The calculated in-plane lattice constants are $a_0 = 6.92$ Å and $b_0 = 3.82$ Å, in agreement with experimental values of $a_0 = 6.9 \pm 0.1$ Å and $b_0 = 4.0 \pm 0.1$ Å [44]. The spin polarized band structure and partial density of state (PDOS) of monolayer Cr_3Te_6 is obtained by the DFT calculation with HSE hybrid functional, as shown in Fig. 1(c) and 1(d), respectively. It is a ferromagnetic metal.

To study the effect of element replacement in the monolayer $(\text{Cr}, \text{Mo})_3\text{Te}_6$, a $1 \times 2 \times 1$ supercell of Cr_3Te_6 is considered, including 6 Cr atoms. In the supercell, 1 and 2 of 6 Cr atoms are replaced by Mo atoms, corresponding to concentration x of 1/6 and 2/6 in $(\text{Cr}_{1-x}, \text{Mo}_x)_3\text{Te}_6$, respectively. The top and side views of structure of monolayer $(\text{Cr}_{4/6}, \text{Mo}_{2/6})_3\text{Te}_6$ is shown in Figs. 1(e) and

1(f), respectively, where 2 of 6 Cr atoms are replaced by Mo atoms. For the monolayer $(\text{Cr}_{1-x}, \text{Mo}_x)_3\text{Te}_6$ with a fixed x , all the possible configurations are considered, and the configuration with the lowest energy is taken as the most stable configuration. The detailed discussion on different configurations is given in Supplemental Material [71]. For the most stable configuration of monolayer $(\text{Cr}_{4/6}, \text{Mo}_{2/6})_3\text{Te}_6$, as shown in Fig. 1(d), the optimized lattice constants are $a = 6.85$ Å and $b = 8.01$ Å, corresponding to in-plane strain of -1.0% and 4.7% along x and y axis, respectively, for the host monolayer Cr_3Te_6 . Significant structural distortion appears due to element replacement. The spin polarized band structure and PDOS of monolayer $(\text{Cr}_{4/6}, \text{Mo}_{2/6})_3\text{Te}_6$ are obtained by the DFT calculation with HSE hybrid functional, as shown in Fig. 1(g) and 1(h). It is a ferromagnetic semiconductor with a band gap of 0.34 eV. Therefore, by replacing 2/6 of Cr atoms with Mo atoms in monolayer Cr_3Te_6 , the ferromagnetic semiconductor $(\text{Cr}_{4/6}, \text{Mo}_{2/6})_3\text{Te}_6$ is obtained.

To study the structural stability, the formation energy $E_{\text{formation}}$ of monolayer $(\text{Cr}_{1-x}, \text{Mo}_x)_3\text{Te}_6$ is calculated by

$$E_{\text{formation}} = \frac{E_{(\text{Cr}_{1-x}, \text{Mo}_x)_3\text{Te}_6} - 3(1-x)E_{\text{Cr}} - 3xE_{\text{Mo}} - 6E_{\text{Te}}}{9}, \quad (1)$$

where $E_{(\text{Cr}_{1-x}, \text{Mo}_x)_3\text{Te}_6}$ is the energy of monolayer $(\text{Cr}_{1-x}, \text{Mo}_x)_3\text{Te}_6$. E_{Cr} and E_{Mo} are energies per atom

for bulks of Cr and Mo with space group $\text{Im}\bar{3}\text{m}$. The formation energies are -0.84 eV/atom and -0.62 eV/atom for monolayers Cr_3Te_6 and $(\text{Cr}_{4/6}, \text{Mo}_{2/6})_3\text{Te}_6$, respectively, indicating their stability.

The defect formation energy $E_{\text{d.f.}}$ of Mo in $(\text{Cr}_{1-x}, \text{Mo}_x)_3\text{Te}_6$ is given by [56]

$$E_{\text{d.f.}} = \frac{E_{(\text{Cr}_{1-x}, \text{Mo}_x)_3\text{Te}_6} - E_{\text{Cr}_3\text{Te}_6}}{x} + 3E_{\text{Cr}} - 3E_{\text{Mo}}, \quad (2)$$

where $E_{\text{Cr}_3\text{Te}_6}$ is the energy of monolayer Cr_3Te_6 , and the other terms are the same in Eq. (1). The defect formation energy $E_{\text{d.f.}}$ shows the change of energy of Cr_3Te_6 per Mo atom. The calculated defect formation energy of Cd in monolayer $(\text{Cr}_{1-x}, \text{Mo}_x)_3\text{Te}_6$ is -5.18 eV per Mo atom, which means that there is an energy reduction of 5.18 eV per Mo atom, and indicates the feasibility of replacing Cr atoms with Mo atoms in monolayer Cr_3Te_6 .

In addition, we performed molecular dynamics simulations of monolayer $(\text{Cr}_{1-x}, \text{Mo}_x)_3\text{Te}_6$ at 300 K, taking the NVT ensemble and running for 6 ps [72]. The results show that monolayer $(\text{Cr}_{1-x}, \text{Mo}_x)_3\text{Te}_6$ is thermodynamically stable [71].

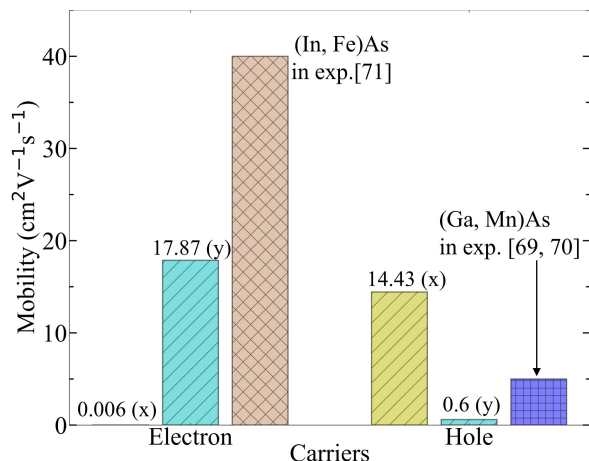


FIG. 2. The calculated results of mobility for $(\text{Cr}_{4/6}, \text{Mo}_{2/6})_3\text{Te}_6$ and the experimental results of hole mobility of (Ga, Mn)As [73, 74], and electron mobility of (In, Fe)As [75].

The mobility of monolayer $(\text{Cr}_{1-x}, \text{Mo}_x)_3\text{Te}_6$ were calculated based on deformation potential theory [76]. The calculated results of mobility for $(\text{Cr}_{4/6}, \text{Mo}_{2/6})_3\text{Te}_6$ by Perdew-Burke-Ernzerhof (PBE) exchange-correlation potential [77] is shown in Fig. 2, show an anisotropic mobility. Elections show a mobility of $17.87 \text{ cm}^2\text{V}^{-1}\text{s}^{-1}$ along y direction and a small mobility of $0.006 \text{ cm}^2\text{V}^{-1}\text{s}^{-1}$ along x direction. Holes show a mobility of $14.63 \text{ cm}^2\text{V}^{-1}\text{s}^{-1}$ along x direction and a small mobility of $0.6 \text{ cm}^2\text{V}^{-1}\text{s}^{-1}$ along y direction. Holes and electrons exhibit high mobility in x and y directions, respectively, while the mobility in another direction is nearly negligible. $(\text{Cr}_{4/6}, \text{Mo}_{2/6})_3\text{Te}_6$ shows considerable mobility

compared with FM semiconductors in experiments. The hole mobility of (Ga, Mn)As is about $10 \text{ cm}^2\text{V}^{-1}\text{s}^{-1}$ and the electron mobility in (In, Fe)As is tens of $\text{cm}^2\text{V}^{-1}\text{s}^{-1}$ [73–75]. Details are shown in Supplemental Material [71].

To study the magnetic properties of monolayer $(\text{Cr}_{4/6}, \text{Mo}_{2/6})_3\text{Te}_6$, we consider a 2D Heisenberg-type Hamiltonian, which can be written as

$$H = J_{\parallel} \sum_{\langle i,j \rangle}^{\text{interlayer}} \vec{S}_i \cdot \vec{S}_j + J_{\perp} \sum_{\langle i,j \rangle}^{\text{intralayer}} \vec{S}_i \cdot \vec{S}_j + A \sum_i S_{iz}^2, \quad (3)$$

where \vec{S}_i and \vec{S}_j are spin operators of magnetic atoms at site i and j , respectively. J_{\parallel} and J_{\perp} are the exchange coupling constants between the nearest-neighbor interlayer and intralayer magnetic atoms, respectively. The single-ion magnetic anisotropy parameter A is obtained by $AS^2 = (E_{\perp} - E_{\parallel}) / (N_{\text{Cr}} + N_{\text{Mo}})$, where N_{Cr} and N_{Mo} are numbers of Cr and Mo atoms in $(\text{Cr}_{4/6}, \text{Mo}_{2/6})_3\text{Te}_6$, respectively. E_{\perp} and E_{\parallel} are energies of $(\text{Cr}_{4/6}, \text{Mo}_{2/6})_3\text{Te}_6$ with out-of-plane and in-plane magnetization, respectively. By DFT results, AS^2 is calculated to be 0.95 meV/atom .

For the monolayer $(\text{Cr}_{4/6}, \text{Mo}_{2/6})_3\text{Te}_6$, a FM, an AFM and a ferrimagnetic (FIM) spin configurations are considered, as shown in Figs. 3(e), 3(f) and 3(g), respectively. Their energies can be expressed as $E_{\text{FM}} = J_{\parallel} (4S_{\text{Cr}}^2 + 8S_{\text{Cr}}S_{\text{Mo}} + 2S_{\text{Mo}}^2) + J_{\perp} (S_{\text{Cr}}^2 + S_{\text{Cr}}S_{\text{Mo}}) + E_0$, $E_{\text{AFM}} = J_{\parallel} (-4S_{\text{Cr}}^2 - 2S_{\text{Mo}}^2) + J_{\perp} (S_{\text{Cr}}^2 + S_{\text{Cr}}S_{\text{Mo}}) + E_0$, $E_{\text{FIM}} = J_{\parallel} (2S_{\text{Cr}}^2 + 8S_{\text{Cr}}S_{\text{Mo}} + 2S_{\text{Mo}}^2) - J_{\perp} (S_{\text{Cr}}^2 + S_{\text{Cr}}S_{\text{Mo}}) + E_0$, where S_{Cr} and S_{Mo} are magnetic moments of Cr and Mo atoms, respectively. E_0 is the energy part independent of spin configurations, which is included in the total energy of DFT results for $(\text{Cr}_{4/6}, \text{Mo}_{2/6})_3\text{Te}_6$. The DFT results show $S_{\text{Cr}} = 3.645 \mu_{\text{B}}$ and $S_{\text{Mo}} = 2.264 \mu_{\text{B}}$ in the supercell $(\text{Cr}_{4/6}, \text{Mo}_{2/6})_3\text{Te}_6$. The exchange coupling parameters of $(\text{Cr}_{4/6}, \text{Mo}_{2/6})_3\text{Te}_6$ can be calculated by $J_{\parallel} = (E_{\text{FM}} - E_{\text{AFM}}) / (8S_{\text{Cr}}^2 + 8S_{\text{Cr}}S_{\text{Mo}} + 4S_{\text{Mo}}^2)$, $J_{\perp} = (E_{\text{FM}} - E_{\text{FIM}}) / (2S_{\text{Cr}}^2 + 2S_{\text{Cr}}S_{\text{Mo}})$. The DFT results with HSE hybrid functional for relative total energy of monolayer $(\text{Cr}_{4/6}, \text{Mo}_{2/6})_3\text{Te}_6$ in FM, AFM and FIM states are 0, 684 and 304 meV, respectively. The exchange coupling constants can be calculated as $J_{\parallel} = -3.55 \text{ meV}$, $J_{\perp} = -7.05 \text{ meV}$. By the Monte Carlo simulation based on the 2D Heisenberg model in Eq. (3), the temperature dependent magnetization and susceptibility of monolayer $(\text{Cr}_{4/6}, \text{Mo}_{2/6})_3\text{Te}_6$ are calculated, as shown in Fig. 3(h). The Curie temperature is estimated as $T_{\text{C}} = 400 \text{ K}$, higher than that of monolayer Cr_3Te_6 . The calculation results show that the monolayer $(\text{Cr}_{4/6}, \text{Mo}_{2/6})_3\text{Te}_6$ is a ferromagnetic semiconductor with band gap of 0.34 eV and T_{C} of 400 K .

For monolayer Cr_3Te_6 , spin configurations in Figs. 3(a)-(c) are considered. Taking $S_{\text{Mo}} = S_{\text{Cr}}$, we obtain $E_{\text{FM}} = (14J_{\parallel} + 2J_{\perp}) S_{\text{Cr}}^2 + E_0$, $E_{\text{AFM}} =$

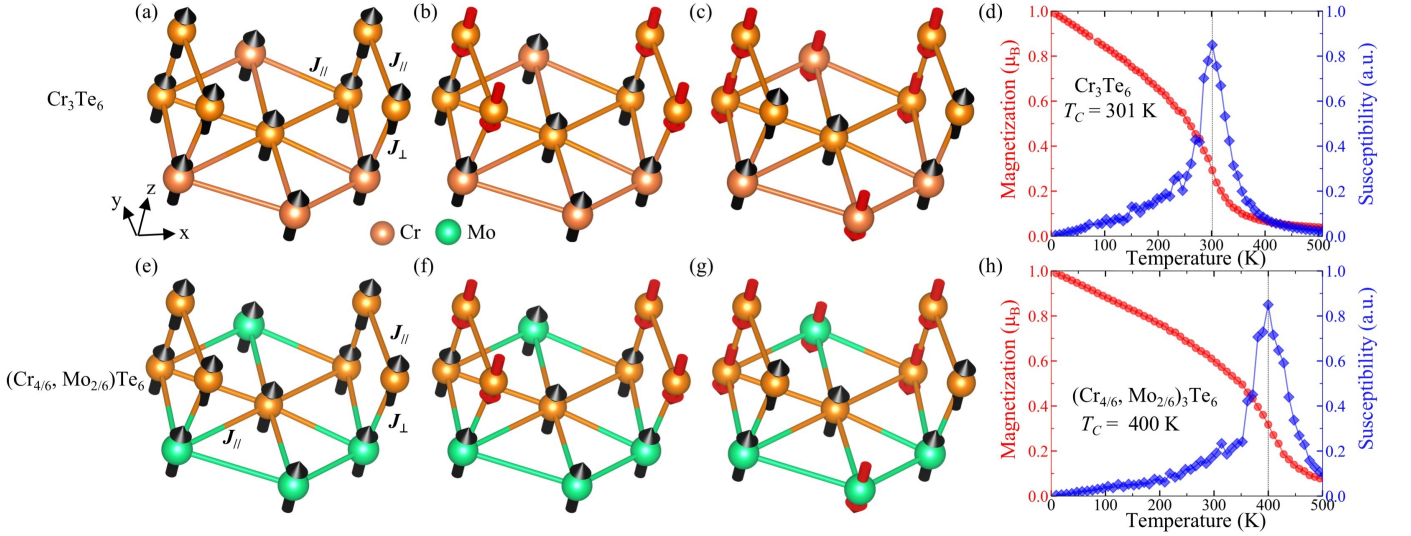


FIG. 3. Spin configurations and magnetic properties of monolayers Cr_3Te_6 and $(\text{Cr}_{4/6}, \text{Mo}_{2/6})_3\text{Te}_6$. A ferromagnetic (FM) (a), an antiferromagnetic (AFM) (b) and a ferrimagnetic (c) spin configurations are considered to get exchange coupling parameters J_{\parallel} and J_{\perp} of Cr_3Te_6 . A ferromagnetic (FM) (e), an antiferromagnetic (AFM) (f) and a ferrimagnetic (g) spin configurations are considered for $(\text{Cr}_{4/6}, \text{Mo}_{2/6})_3\text{Te}_6$. Magnetization and susceptibility of Cr_3Te_6 (d) and $(\text{Cr}_{4/6}, \text{Mo}_{2/6})_3\text{Te}_6$ (e) as functions of temperature, obtained by the Monte Carlo simulations based on the 2D Heisenberg model. T_C of monolayers Cr_3Te_6 and $(\text{Cr}_{4/6}, \text{Mo}_{2/6})_3\text{Te}_6$ are calculated as 301 K and 400 K, respectively. It is noted that $T_C = 344$ K for monolayer Cr_3Te_6 in experiment [44].

$(-6J_{\parallel} + 2J_{\perp})S_{\text{Cr}}^2 + E_0$, $E_{\text{FIM}} = (14J_{\parallel} - 2J_{\perp})S_{\text{Cr}}^2 + E_0$, and $J_{\parallel} = (E_{\text{FM}} - E_{\text{AFM}})/(20S_{\text{Cr}}^2)$, $J_{\perp} = (E_{\text{FM}} - E_{\text{FIM}})/(4S_{\text{Cr}}^2)$. The DFT results with HSE hybrid functional for relative total energy of monolayer Cr_3Te_6 in FM, AFM and FIM states are 0, 454 and 273 meV, respectively, giving $J_{\parallel}S_{\text{Cr}}^2 = -22.7$ meV and $J_{\perp}S_{\text{Cr}}^2 = -68.1$ meV. The magnetic moment $S_{\text{Cr}} = 3.50 \mu_{\text{B}}$ in monolayer Cr_3Te_6 , therefore the exchange coupling constants of monolayer Cr_3Te_6 can be calculated as $J_{\parallel} = -1.85$ meV and $J_{\perp} = -5.55$ meV. The single-ion magnetic anisotropy energy of monolayer Cr_3Te_6 is calculated to be $AS^2 = 0.91$ meV/Cr. The Monte Carlo simulation result gives $T_C = 301$ K of monolayer Cr_3Te_6 , as shown in Fig. 3 (d). It is noted that for the monolayer Cr_3Te_6 , the calculated T_C is lower than the experimental $T_C = 344$ K [44].

Properties of monolayers $(\text{Cr}, \text{D})_3\text{Te}_6$ and $(\text{Mn}, \text{D})\text{Se}_2$.—In the similar way, we have studied the monolayers $(\text{Cr}, \text{D})_3\text{Te}_6$ and $(\text{Mn}, \text{D})\text{Se}_2$, where element D is taken as vacancy, 3d, 4d, 5d transitional metal elements. We considered a supercell of $1 \times 2 \times 1$ Cr_3Te_6 with 6 Cr atoms. 1 and 2 of 6 Cr atoms are replaced by element D, corresponding to concentration x as $1/6$ and $2/6$ in $(\text{Cr}_{1-x}, \text{D}_x)_3\text{Te}_6$, respectively. HSE hybrid functional approach is used to obtain the band gaps and coupling constants [78]. As shown in Tab. I, some high T_C ferromagnetic semiconductors are predicted, such as $(\text{Cr}_{5/6}, \text{D}_{1/6})_3\text{Te}_6$ with D as W, Tc and Pd, and $(\text{Cr}_{4/6}, \text{D}_{2/6})_3\text{Te}_6$ with D as Pd, Ag, Hg and Mo with T_C above 200 K.

We considered a supercell of $3 \times 3 \times 1$ MnSe_2 with 9 Mn atoms. 1, 2 and 3 of 9 Mn atoms are replaced by element D, corresponding to concentration x of $1/9$, $2/9$ and $3/9$ in $(\text{Mn}_{1-x}, \text{D}_x)\text{Se}_2$, respectively. The obtained ferromagnetic semiconductors of $(\text{Mn}, \text{D})\text{Se}_2$ are shown in Table I, where element D is nonmagnetic. J_{\parallel} in Table I is the nearest in-plane coupling constants in $(\text{Mn}, \text{D})\text{Se}_2$. Some high T_C ferromagnetic semiconductors are predicted, such as monolayers $(\text{Mn}_{6/9}, \text{D}_{3/9})\text{Se}_2$ with D as Mn vacancy, Cd and Au with T_C higher than 200 K. In addition, the band gap of $(\text{Mn}_{1-x}, \text{D}_x)\text{Se}_2$ with D as Mn vacancy increase from 0.07 eV as $x = 2/9$ to 0.64 eV as $x = 3/9$. This behavior has been observed in 2D semimetal gray arsenene, whose band gap increases with the increase of vacancy concentrations [67].

As shown in Tab. I, the obtained 2D ferromagnetic semiconductors show negative formation energies and defect formation energies, indicating their structural stability and feasibility of element replacement. Details of different configurations are given in Supplemental Material [71].

The results in Tab. I predict about 10 ferromagnetic semiconductors with T_C above 200 K, including $(\text{Cr}_{5/6}, \text{W}_{1/6})_3\text{Te}_6$ and $(\text{Cr}_{4/6}, \text{Mo}_{2/6})_3\text{Te}_6$ with T_C above 300 K through element replacement in 2D ferromagnetic metals MnSe_2 and Cr_3Te_6 .

The properties of monolayers $\text{Mn}(\text{Se}, \text{D})_2$ and $\text{Cr}_3(\text{Te}, \text{D})_6$ are also discussed. All results of $\text{Cr}_3(\text{Te}, \text{D})_6$ are metallic. $\text{Mn}(\text{Se}_{6/8}, \text{Sb}_{2/8})_2$ is found to be a ferromagnetic semiconductor with T_C of 330 K and band gap of

TABLE I. The band gap, formation energy $E_{\text{formation}}$, defect formation energy $E_{\text{d.f.}}$, coupling constants, MAE and Curie temperature T_C for monolayers $(\text{Mn}_{1-x}, \text{D}_x)\text{Se}_2$ and $(\text{Cr}_{1-x}, \text{D}_x)_3\text{Te}_6$. Element D is considered as vacancy, 3d, 4d and 5d transitional metal elements with different magnetic moments M_D , and only the results with band gap is shown in the table. The results are obtained by density functional theory calculations and Monte Carlo simulations.

Ferromagnetic Semiconductors				Properties								
Monolayers	x	Element D		Gap (eV)		$E_{\text{d.f.}}$ (eV/D)	$E_{\text{formation}}$ (eV/atom)	J (meV)		MAE (meV)	T_C (K)	
		type	M_D (μ_B)	PBE	HSE			J_{\parallel}	J_{\perp}			
$(\text{Cr}_{1-x}, \text{D}_x)_3\text{Te}_6$	1/6	W	1.16	0	0.15	-12.04	-0.67	-3.37	-4.85	-1.92	362	
		Tc	1.79	0	0.02	-13.11	-0.73	-1.50	-1.70	0.71	222	
		Pd	0	0	0.02	-13.15	-0.73	-2.72	-3.23	0.55	245	
	2/6	Ta			0.14	0.50	-5.98	-0.66	-1.52	-2.53	0.79	71
		Hf			0.09	0.42	-7.58	-0.84	-1.49	-5.23	1.06	103
		Pd			0	0.15	-5.87	-0.65	-2.82	-0.10	-0.47	230
		Pt	0		0.17	0.45	-6.07	-0.67	-1.50	-2.48	1.50	71
		Ag	0		0.13	0.35	-4.91	-0.55	-2.64	/	0.91	217
		Au	0		0	0.03	-5.01	-0.56	-1.96	-0.59	-0.48	159
		Zr	0		0	0.12	-7.71	-0.86	-2.57	-0.56	1.29	198
		Hg	0		0.09	0.33	6.38	0.71	-2.89	/	0.34	220
		Tc	2.75		0.10	0.35	-5.45	-0.61	-1.40	-2.20	0.32	182
	Mo	2.26		0.06	0.34	-5.56	-0.62	-2.95	-6.16	1.74	400	
	Ni	0.83		0	0.07	-5.50	-0.61	-2.64	-6.89	0.67	175	
	$(\text{Mn}_{1-x}, \text{D}_x)\text{Se}_2$	2/9	Mn Vac.	0	0	0.07	-4.48	-0.67	-1.61	/	-1.28	145
3/9		Mn Vac.		0.28	0.64	-2.93	-0.37	-2.93		-0.20	252	
		Nb			0	0.19	-6.03	-0.67	-2.24		0.13	194
		Cd	0		0.25	0.56	-3.53	-0.39	-3.30		1.13	276
		W			0.02	0.19	-4.37	-0.49	-1.09	/	-0.14	94
		Au			0	0.13	-2.85	-0.32	-2.03		-1.07	92
		Hg			0.09	0.38	-2.77	-0.31	-3.08		1.06	226
		Re	1.62		0.33	0.33	-3.62	-0.40	-0.90		-1.11	59

0.26 eV. In addition, $\text{Mn}(\text{Se}_{6/8}, \text{D}_{2/8})_2$ are found to be AFM semiconductors when D is Si, Ge and Sn, with Neel temperatures T_N of 153 K, 224 K and 208 K, respectively. $\text{Mn}(\text{Se}_{5/8}, \text{D}_{3/8})_2$ with D as Si is AFM semiconductor with T_N of 86 K, and FM semiconductors with T_C of 181 K and 94 K when D is Ge and Sn. The details are given in Supplemental Material [71].

Conclusion.—Inspired by the recent experimental progress on 2D metals, such as high Curie temperature T_C above room temperature and doping induced metal-semiconductor transition, we have theoretically studied the possible high T_C ferromagnetic semiconductors by element replacement in 2D ferromagnetic metals. For the 2D materials $(\text{Mn}, \text{D})\text{Se}_2$ and $(\text{Cr}, \text{D})_3\text{Te}_6$ with D being vacancy, 3d, 4d and 5d transitional metal elements and concentration of D from 1/9 to 1/3, we found about 10 ferromagnetic semiconductors with T_C above 200 K, including $(\text{Cr}_{5/6}, \text{W}_{1/6})_3\text{Te}_6$ and $(\text{Cr}_{4/6}, \text{Mo}_{2/6})_3\text{Te}_6$ with T_C above 300 K. In addition, $\text{Mn}(\text{Se}_{6/8}, \text{Sb}_{2/8})_2$ is also found to be a 2D ferromagnetic semiconductor with T_C above 300 K. The calculation results of formation energy and defect formation energy indicate their structural stability and feasibility of the element replacement approach. Our theoretical results demonstrate a way to obtain high temperature ferromagnetic semiconductors from experimentally obtained 2D high T_C ferromagnetic

metals through element replacement, and will simulate further research on high temperature ferromagnetic semiconductors.

Acknowledgements.—This work is supported by National Key R&D Program of China (Grant No. 2022YFA1405100), National Natural Science Foundation of China (Grant No. 12074378), Chinese Academy of Sciences (Grants No. YSBR-030, No. JZHKYPT-2021-08, No. XDB33000000).

* gsu@ucas.ac.cn

† gubo@ucas.ac.cn

- [1] T. Dietl, A ten-year perspective on dilute magnetic semiconductors and oxides, *Nat. Mater.* **9**, 965 (2010).
- [2] H. Ohno, A window on the future of spintronics, *Nat. Mater.* **9**, 952 (2010).
- [3] K. Sato, L. Bergqvist, J. Kudrnovský, P. H. Dederichs, O. Eriksson, I. Turek, B. Sanyal, G. Bouzerar, H. Katayama-Yoshida, V. A. Dinh, T. Fukushima, H. Kizaki, and R. Zeller, First-principles theory of dilute magnetic semiconductors, *Rev. Mod. Phys.* **82**, 1633 (2010).
- [4] T. Jungwirth, J. Sinova, J. Mašek, J. Kučera, and A. H. MacDonald, Theory of ferromagnetic (III, Mn)V semiconductors, *Rev. Mod. Phys.* **78**, 809 (2006).
- [5] T. Dietl and H. Ohno, Dilute ferromagnetic semiconduc-

- tors: Physics and spintronic structures, *Rev. Mod. Phys.* **86**, 187 (2014).
- [6] H. Ohno, Making nonmagnetic semiconductors ferromagnetic, *Science* **281**, 951 (1998).
- [7] H. Kalita, M. Bhushan, and L. R. Singh, A comprehensive review on theoretical concepts, types and applications of magnetic semiconductors, *Mater. Sci. Eng. B: Solid-State Mater. Adv. Technol.* **288**, 116201 (2023).
- [8] M. Fang and E.-H. Yang, Advances in two-dimensional magnetic semiconductors via substitutional doping of transition metal dichalcogenides, *Materials* **16**, 3701 (2023).
- [9] A. Teletin and Y. Sukhorukov, Magnetic semiconductors as materials for spintronics, *Magnetochemistry* **8**, 173 (2022).
- [10] M. Holub, J. Shin, S. Chakrabarti, and P. Bhattacharya, Electrically injected spin-polarized vertical-cavity surface-emitting lasers, *Appl. Phys. Lett.* **87**, 091108 (2005).
- [11] R. Fiederling, M. Keim, G. Reuscher, W. Ossau, G. Schmidt, A. Waag, and L. W. Molenkamp, Injection and detection of a spin-polarized current in a light-emitting diode, *Nature* **402**, 787 (1999).
- [12] N. I. Solin, S. V. Naumov, and A. A. Samokhvalov, Interface phenomena and microwave magnetoresistance in polycrystalline $\text{La}_{1-x}\text{Ca}_x\text{MnO}_3$ lanthanum manganites, *Phys. Solid State* **42**, 925 (2000).
- [13] H. Ohno, D. Chiba, F. Matsukura, T. Omiya, E. Abe, T. Dietl, Y. Ohno, and K. Ohtani, Electric-field control of ferromagnetism, *Nature* **408**, 944 (2000).
- [14] C. Mitra, P. Raychaudhuri, G. Köbernik, K. Dörr, K.-H. Müller, L. Schultz, and R. Pinto, p-n diode with hole- and electron-doped lanthanum manganites, *Appl. Phys. Lett.* **79**, 2408 (2001).
- [15] N. Bebenin and V. Ustinov, Inverse spin population near ferromagnet/nonmagnetic semiconductor contact, *J. Magn. Magn. Mater.* **272–276**, 1917 (2004).
- [16] X. Li, J.-T. Lü, J. Zhang, L. You, Y. Su, and E. Y. Tsymbal, Spin-dependent transport in van der Waals magnetic tunnel junctions with Fe_3GeTe_2 electrodes, *Nano Lett.* **19**, 5133 (2019).
- [17] T. Song, X. Cai, M. W.-Y. Tu, X. Zhang, B. Huang, N. P. Wilson, K. L. Seyler, L. Zhu, T. Taniguchi, K. Watanabe, M. A. McGuire, D. H. Cobden, D. Xiao, W. Yao, and X. Xu, Giant tunneling magnetoresistance in spin-filter van der Waals heterostructures, *Science* **360**, 1214 (2018).
- [18] O. Gorbenko, A. Kaul, O. Mel'nikov, E. Gan'shina, A. Ganin, Y. Sukhorukov, N. Loshkareva, and E. Mostovshchikova, Synthetic routes to colossal magnetoresistance manganites thin films containing unstable or highly volatile metal oxides, *Thin Solid Films* **515**, 6395 (2007).
- [19] S. Goel, N. H. D. Khang, Y. Osada, L. D. Anh, P. N. Hai, and M. Tanaka, Room-temperature spin injection from a ferromagnetic semiconductor, *Sci. Rep.* **13**, 10.1038/s41598-023-29169-9 (2023).
- [20] M. Cinchetti, K. Heimer, J.-P. Wüstenberg, O. Andreyev, M. Bauer, S. Lach, C. Ziegler, Y. Gao, and M. Aeschlimann, Determination of spin injection and transport in a ferromagnet/organic semiconductor heterojunction by two-photon photoemission, *Nat. Mater.* **8**, 115 (2008).
- [21] P. K. Baltzer, P. J. Wojtowicz, M. Robbins, and E. Lopatin, Exchange interactions in ferromagnetic chromium chalcogenide spinels, *Phys. Rev.* **151**, 367 (1966).
- [22] B. Huang, G. Clark, E. Navarro-Moratalla, D. R. Klein, R. Cheng, K. L. Seyler, D. Zhong, E. Schmidgall, M. A. McGuire, D. H. Cobden, W. Yao, D. Xiao, P. Jarillo-Herrero, and X. Xu, Layer-dependent ferromagnetism in a van der Waals crystal down to the monolayer limit, *Nature* **546**, 270 (2017).
- [23] C. Gong, L. Li, Z. Li, H. Ji, Alex Stern, Y. Xia, T. Cao, W. Bao, C. Wang, Y. Wang, Z. Q. Qiu, R. J. Cava, S. G. Louie, J. Xia, and X. Zhang, Discovery of intrinsic ferromagnetism in two-dimensional van der Waals crystals, *Nature* **546**, 265 (2017).
- [24] N. D. Mermin and H. Wagner, Absence of ferromagnetism or antiferromagnetism in one- or two-dimensional isotropic Heisenberg models, *Phys. Rev. Lett.* **17**, 1307 (1966).
- [25] J. Chu, Y. Zhang, Y. Wen, R. Qiao, C. Wu, P. He, L. Yin, R. Cheng, F. Wang, Z. Wang, J. Xiong, Y. Li, and J. He, Sub-millimeter-scale growth of one-unit-cell-thick ferromagnetic Cr_2S_3 nanosheets, *Nano Lett.* **19**, 2154 (2019).
- [26] X. Cai, T. Song, N. P. Wilson, G. Clark, M. He, X. Zhang, T. Taniguchi, K. Watanabe, W. Yao, D. Xiao, M. A. McGuire, D. H. Cobden, and X. Xu, Atomically thin CrCl_3 : An in-plane layered antiferromagnetic insulator, *Nano Lett.* **19**, 3993 (2019).
- [27] Z. Zhang, J. Shang, C. Jiang, A. Rasmita, W. Gao, and T. Yu, Direct photoluminescence probing of ferromagnetism in monolayer two-dimensional CrBr_3 , *Nano Lett.* **19**, 3138 (2019).
- [28] B. Achinuq, R. Fujita, W. Xia, Y. Guo, P. Bencok, G. van der Laan, and T. Hesjedal, Covalent mixing in the 2D ferromagnet CrSiTe_3 evidenced by magnetic X-ray circular dichroism, *Phys. Status. Solidi.* **16**, 2100566 (2021).
- [29] K. Lee, A. H. Dismukes, E. J. Telford, R. A. Wisconsin, J. Wang, X. Xu, C. Nuckolls, C. R. Dean, X. Roy, and X. Zhu, Magnetic order and symmetry in the 2D semiconductor CrSBr , *Nano Lett.* **21**, 3511 (2021).
- [30] J.-Y. You, X.-J. Dong, B. Gu, and G. Su, Possible room-temperature ferromagnetic semiconductors, *Chin. Phys. Lett.* **40**, 067502 (2023).
- [31] X.-J. Dong, J.-Y. You, B. Gu, and G. Su, Strain-induced room-temperature ferromagnetic semiconductors with large anomalous Hall conductivity in two-dimensional $\text{Cr}_2\text{Ge}_2\text{Se}_6$, *Phys. Rev. Appl.* **12**, 014020 (2019).
- [32] J.-Y. You, Z. Zhang, B. Gu, and G. Su, Two-dimensional room-temperature ferromagnetic semiconductors with Quantum anomalous Hall effect, *Phys. Rev. Appl.* **12**, 024063 (2019).
- [33] J.-Y. You, Z. Zhang, X.-J. Dong, B. Gu, and G. Su, Two-dimensional magnetic semiconductors with room curie temperatures, *Phys. Rev. Res.* **2**, 013002 (2020).
- [34] C. Huang, J. Feng, J. Zhou, H. Xiang, K. Deng, and E. Kan, Ultra-high-temperature ferromagnetism in intrinsic tetrahedral semiconductors, *JACS* **141**, 12413 (2019).
- [35] Z. Jiang, P. Wang, J. Xing, X. Jiang, and J. Zhao, Screening and design of novel 2D ferromagnetic materials with high Curie temperature above room temperature, *ACS Appl. Mater. Interfaces* **10**, 39032 (2018).
- [36] C. Huang, J. Feng, F. Wu, D. Ahmed, B. Huang, H. Xiang, K. Deng, and E. Kan, Toward intrinsic room-

- temperature ferromagnetism in two-dimensional semiconductors, *JACS* **140**, 11519 (2018).
- [37] J.-W. Li, Z. Zhang, J.-Y. You, B. Gu, and G. Su, Two-dimensional Heisenberg model with material-dependent superexchange interactions, *Phys. Rev. B* **107**, 224411 (2023).
- [38] S. Chen, F. Wu, Q. Li, H. Sun, J. Ding, C. Huang, and E. Kan, Prediction of room-temperature ferromagnetism in a two-dimensional direct band gap semiconductor, *Nanoscale* **12**, 15670 (2020).
- [39] G. Song, D. Li, H. Zhou, C. Zhang, Z. Li, G. Li, B. Zhang, X. Huang, and B. Gao, Intrinsic room-temperature ferromagnetic semiconductor InCrTe₃ monolayers with large magnetic anisotropy and large piezoelectricity, *Appl. Phys. Lett.* **118**, 10.1063/5.0043731 (2021).
- [40] H. Wang, S. Sun, J. Lu, J. Xu, X. Lv, Y. Peng, X. Zhang, Y. Wang, and G. Xiang, High curie temperature ferromagnetism and high hole mobility in tensile strained Mn-doped SiGe thin films, *Adv. Funct. Mater.* **30**, 2002513 (2020).
- [41] X. Zhang, Q. Lu, W. Liu, W. Niu, J. Sun, J. CoOk, M. Vaninger, P. F. Miceli, D. J. Singh, S.-W. Lian, T.-R. Chang, X. He, J. Du, L. He, R. Zhang, G. Bian, and Y. Xu, Room-temperature intrinsic ferromagnetism in epitaxial CrTe₂ ultrathin films, *Nat. Commun.* **12**, 2492 (2021).
- [42] J.-J. Xian, C. Wang, J.-H. Nie, R. Li, M. Han, J. Lin, W.-H. Zhang, Z.-Y. Liu, Z.-M. Zhang, M.-P. Miao, Y. Yi, S. Wu, X. Chen, J. Han, Z. Xia, W. Ji, and Y.-S. Fu, Spin mapping of intralayer antiferromagnetism and field-induced spin reorientation in monolayer CrTe₂, *Nat. Commun.* **13**, 13:257 (2022).
- [43] D. Wang, X. Wang, B. Hu, J. Wang, Y. Zou, J. Guo, Z. Li, S. Wang, Y. Li, G. Song, H. Wang, and Y. Liu, Strain- and electron doping-induced in-plane spin orientation at room temperature in single-layer CrTe₂, *ACS Appl. Mater. Interfaces* , 28791 (2024).
- [44] R. Chua, J. Zhou, X. Yu, W. Yu, J. Gou, R. Zhu, L. Zhang, M. Liu, M. B. H. Breese, W. Chen, K. P. Loh, Y. P. Feng, M. Yang, Y. L. Huang, and A. T. S. Wee, Room temperature ferromagnetism of monolayer chromium telluride with perpendicular magnetic anisotropy, *Adv. Mater.* **33**, 2103360 (2021).
- [45] B. Li, X. Deng, W. Shu, X. Cheng, Q. Qian, Z. Wan, B. Zhao, X. Shen, R. Wu, S. Shi, H. Zhang, Z. Zhang, X. Yang, J. Zhang, M. Zhong, Q. Xia, J. Li, Y. Liu, L. Liao, Y. Ye, L. Dai, Y. Peng, B. Li, and X. Duan, Air-stable ultrathin Cr₃Te₄ nanosheets with thickness-dependent magnetic skyrmions, *Mater. Today* **57**, 66 (2022).
- [46] Y. Zhang, J. Chu, L. Yin, T. Shifa, Z. Cheng, R. Cheng, F. Wang, Y. Wen, X. Zhan, Z. Wang, and J. He, Ultrathin magnetic 2D single-crystal CrSe, *Adv. Mater.* **31**, 1900056 (2019).
- [47] Y. Deng, Y. Yu, Y. Song, J. Zhang, N. Z. Wang, Z. Sun, Y. Yi, Y. Z. Wu, S. Wu, J. Zhu, J. Wang, X. H. Chen, and Y. Zhang, Gate-tunable room-temperature ferromagnetism in two-dimensional Fe₃GeTe₂, *Nature* **563**, 94 (2018).
- [48] Z. Fei, B. Huang, P. Malinowski, W. Wang, T. Song, J. Sanchez, W. Yao, D. Xiao, X. Zhu, A. F. May, W. Wu, D. H. Cobden, J.-H. Chu, and X. Xu, Two-dimensional itinerant ferromagnetism in atomically thin Fe₃GeTe₂, *Nat. Mater.* **17**, 778 (2018).
- [49] J. Seo, D. Kim, E. An, K. Kim, G.-Y. Kim, S.-Y. Hwang, D. Kim, B. Jang, H. Kim, G. Eom, S. Seo, R. Stania, M. Muntwiler, J. Lee, K. Watanabe, T. Taniguchi, Y. Jo, J. Lee, B. Min, M. Jo, H. Yeom, S.-Y. Choi, J. Shim, and J. Kim, Nearly room temperature ferromagnetism in a magnetic metal-rich van der Waals metal, *Sci. Adv.* **6**, eaay8912 (2020).
- [50] A. May, D. Ovchinnikov, Q. Zheng, R. Hermann, S. Calder, B. Huang, Z. Fei, Y. Liu, X. Xu, and M. McGuire, Ferromagnetism near room temperature in the cleavable van der Waals crystal Fe₅GeTe₂, *ACS Nano* **13**, 4436 (2019).
- [51] G. Zhang, F. Guo, H. Wu, X. Wen, L. Yang, W. Jin, W. Zhang, and H. Chang, Above-room-temperature strong intrinsic ferromagnetism in 2D van der Waals Fe₃GaTe₂ with large perpendicular magnetic anisotropy, *Nat. Commun.* **13**, 5067 (2022).
- [52] Z. Chen, Y. Yang, T. Ying, and J.-g. Guo, High-T_c ferromagnetic semiconductor in thinned 3D Ising ferromagnetic metal Fe₃GaTe₂, *Nano Lett.* **24**, 993 (2024).
- [53] D. O'hara, T. Zhu, A. Trout, A. Ahmed, Y. Luo, C. Lee, M. Brenner, S. Rajan, J. Gupta, D. McComb, and R. Kawakami, Room temperature intrinsic ferromagnetism in epitaxial manganese selenide films in the monolayer limit, *Nano Lett.* **18**, 3125 (2018).
- [54] B. Li, T. Xing, M. Zhong, L. Huang, N. Lei, J. Zhang, J. Li, and Z. Wei, A two-dimensional Fe-doped SnS₂ magnetic semiconductor, *Nat. Commun.* **8**, 8: 1958 (2017).
- [55] D. Shen, B. Zhao, Z. Zhang, H. Zhang, X. Yang, Z. Huang, B. Li, R. Song, Y. Jin, R. Wu, B. Li, J. Li, and X. Duan, Synthesis of Group VIII magnetic transition-metal-doped monolayer MoSe₂, *ACS Nano* **16**, 10623 (2022).
- [56] J. Jiang, W. Feng, Y. Wen, L. Yin, H. Wang, X. Feng, Y. Pei, R. Cheng, and J. He, Tuning 2D magnetism in cobalt monoxide nanosheets via in situ nickel-doping, *Adv. Mater.* **35**, 2301668 (2023).
- [57] F. Zhang, B. Zheng, A. Sebastian, D. H. Olson, M. Liu, K. Fujisawa, Y. T. H. Pham, V. O. Jimenez, V. Kalappattil, L. Miao, T. Zhang, R. Pendurthi, Y. Lei, A. L. Elías, Y. Wang, N. Alem, P. E. Hopkins, S. Das, V. H. Crespi, M. Phan, and M. Terrones, Monolayer vanadium-doped tungsten disulfide: A room-temperature dilute magnetic semiconductor, *Adv. Sci.* **7**, 2001174 (2020).
- [58] M. Kar, R. Sarkar, S. Pal, and P. Sarkar, Engineering the magnetic properties of PtSe₂ monolayer through transition metal doping, *J. Phys. Condens. Matter* **31**, 145502 (2019).
- [59] S. Tiwari, M. L. Van de Put, B. Sorée, and W. G. Vandenberghe, Magnetic order and critical temperature of substitutionally doped transition metal dichalcogenide monolayers, *npj 2D Mater. Appl.* **5**, 54 (2021).
- [60] M. Zhang, H.-m. Guo, J. Lv, J.-f. Jia, and H.-s. Wu, The 3d transition-metals doping tunes the electronic and magnetic properties of 2D monolayer InP₃, *J. Magn. Mater.* **533**, 168026 (2021).
- [61] A. Smiri, S. Jaziri, S. Lounis, and I. C. Gerber, DFT+U investigation of magnetocrystalline anisotropy of Mn-doped transition-metal dichalcogenide monolayers, *Phys. Rev. Materials* **5**, 054001 (2021).
- [62] B. D. Bhat, Tuning the magnetic and electronic properties of monolayer SnS₂ by 3d transition metal doping: A DFT study, *Mater. Today Commun.* **33**, 104626 (2022).
- [63] L. Cai, J. He, Q. Liu, T. Yao, L. Chen, W. Yan, F. Hu,

- Y. Jiang, Y. Zhao, T. Hu, Z. Sun, and S. Wei, Vacancy-induced ferromagnetism of MoS₂ nanosheets, *J. Am. Chem. Soc.* **137**, 2622 (2015).
- [64] J. Zhong, X. Zhang, W. He, D. Gong, M. Lan, X. Dai, Y. Peng, and G. Xiang, Large-scale fabrication and Mo vacancy-induced robust room-temperature ferromagnetism of MoSe₂ thin films, *Nanoscale* **15**, 6844 (2023).
- [65] Z. Xiao, H. Huang, S. Hu, Z. Weng, Y. Huang, B. Du, X. Zeng, Y. Meng, and C. Huang, Bifunctional square-planar NiO₄ coordination of topotactic LaNiO_{2.0} films for efficient oxygen evolution reaction, *Small Methods* **8**, 2300793 (2023).
- [66] Y. Zhu, Y. Gao, X. Jiang, and J. Zhao, Effects of vacancy defects on the magnetic properties of vanadium diselenide monolayers: a first principle investigation, *Phys. Chem. Chem. Phys.* **24**, 17615 (2022).
- [67] Y. Hu, X. Wang, Z. Qi, S. Wan, J. Liang, Q. Jia, D. Hong, Y. Tian, J. Ma, Z. Tie, and Z. Jin, Wet chemistry vitrification and metal-to-semiconductor transition of 2D gray arsenene nanoflakes, *Adv. Funct. Mater.* **31**, 2106529 (2021).
- [68] Y. Deng, Z. Xiang, B. Lei, K. Zhu, H. Mu, W. Zhuo, X. Hua, M. Wang, Z. Wang, G. Wang, M. Tian, and X. Chen, Layer-number-dependent magnetism and anomalous Hall effect in van der Waals ferromagnet Fe₅GeTe₂, *Nano Lett.* **22**, 9839 (2022).
- [69] A. Hashmi, T. Hu, and J. Hong, Transition from half metal to semiconductor in Li doped g-C₄N₃, *J. Appl. Phys.* **115**, 115, 124312 (2014).
- [70] H. Liu, Z. Huang, C. He, S. Zhang, Y. Liao, X. Qi, and J. Zhong, Metal-to-semiconductor transitions in constituent-tunable layered two-dimensional Nb W_{1-x}Se₂ based on first principles calculations, *Physica E* **144**, 115388 (2022).
- [71] See supplemental material.
- [72] J.-Y. You, B. Gu, and G. Su, The p-orbital magnetic topological states on a square lattice, *Natl. Sci. Rev.* **9**, nwab114 (2021).
- [73] W. Limmer, A. Koeder, S. Frank, V. Avrutin, W. Schoch, R. Sauer, K. Zuern, J. Eisenmenger, P. Ziemann, E. Peiner, and A. Waag, Effect of annealing on the depth profile of hole concentration in (Ga,Mn)As, *Phys. Rev. B* **71**, 205213 (2005).
- [74] R. Moriya and H. Munekata, Relation among concentrations of incorporated Mn atoms, ionized Mn acceptors, and holes in p-(Ga,Mn)As epilayers, *J. Appl. Phys.* **93**, 4603 (2003).
- [75] M. Tanaka, S. Ohya, and P. Nam Hai, Recent progress in III-V based ferromagnetic semiconductors: Band structure, Fermi level, and tunneling transport, *Appl. Phys. Rev.* **1**, 011102 (2014).
- [76] G. Schusteritsch, M. Uhrin, and C. J. Pickard, Single-layered hitorf's phosphorus: A wide-bandgap high mobility 2D material, *Nano Lett.* **16**, 2975 (2016).
- [77] J. P. Perdew, K. Burke, and M. Ernzerhof, Generalized gradient approximation made simple, *Phys. Rev. Lett.* **77**, 3865 (1996).
- [78] J. Heyd, G. E. Scuseria, and M. Ernzerhof, Hybrid functionals based on a screened Coulomb potential, *J. Chem. Phys.* **118**, 8207 (2003).